



HAL
open science

Syntheses and Structures of Facial and Meridional Stereoisomers of kappa(2)-N,S-Chelated Ruthenium Borate Complexes

Asif Ahmad, Suvam Saha, Mohammad Zafar, Thierry Roisnel, Prasanta Ghosh, Sundargopal Ghosh

► **To cite this version:**

Asif Ahmad, Suvam Saha, Mohammad Zafar, Thierry Roisnel, Prasanta Ghosh, et al.. Syntheses and Structures of Facial and Meridional Stereoisomers of kappa(2)-N,S-Chelated Ruthenium Borate Complexes. *European Journal of Organic Chemistry*, 2023, 26 (9), pp.e202201283. 10.1002/ejoc.202201283 . hal-04057787

HAL Id: hal-04057787

<https://hal.science/hal-04057787>

Submitted on 11 May 2023

HAL is a multi-disciplinary open access archive for the deposit and dissemination of scientific research documents, whether they are published or not. The documents may come from teaching and research institutions in France or abroad, or from public or private research centers.

L'archive ouverte pluridisciplinaire **HAL**, est destinée au dépôt et à la diffusion de documents scientifiques de niveau recherche, publiés ou non, émanant des établissements d'enseignement et de recherche français ou étrangers, des laboratoires publics ou privés.



Distributed under a Creative Commons Attribution - NonCommercial 4.0 International License

Synthesis and Structures of Facial and Meridional Stereoisomers of κ^2 -*N,S*-Chelated Ruthenium Borate Complexes

Asif Ahmad,^[a] Suvam Saha,^{†[a]} Mohammad Zafar,^{†[a]} Thierry Roisnel,^[b] Prasanta Ghosh,^[c] Sundargopal Ghosh*^[a]

[a] Asif Ahmad, Suvam Saha, Mohammad Zafar, Dr. Sundargopal Ghosh
Department of Chemistry
Indian Institute of Technology Madras
Chennai 600036, India
E-mail: sghosh@iitm.ac.in

[b] Dr. Thierry Roisnel
Department of ISCR Instruments
Univ Rennes, CNRS, Institut des Sciences Chimiques de Rennes, UMR 6226, F-35000 Rennes, France

[c] Dr. Prasanta Ghosh
Department of Chemistry
R. K. Mission Residential College, Kolkata 700103, India

† These authors contributed equally to this work

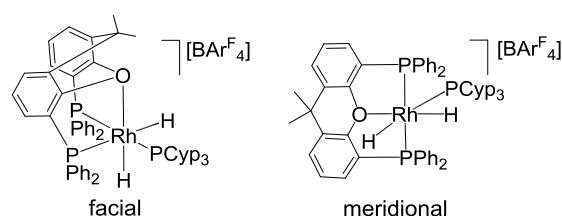
Abstract: The *trans-mer*-[(κ^2 -*N,S*-NS₂C₇H₄)PR₃Ru{ κ^3 -*H,S,S'*-H₂B(NS₂C₇H₄)₂}], (*trans-mer-1a*: R = Cy; *trans-mer-1b*: R = Ph) complexes are kinetically controlled products that upon thermolysis led to the formation of *cis-mer*-[(κ^2 -*N,S*-NS₂C₇H₄)PR₃Ru{ κ^3 -*H,S,S'*-H₂B(NS₂C₇H₄)₂}], (*cis-mer-2a*: R = Cy; *cis-mer-2b*: R = Ph) and *cis-fac*-[(κ^2 -*N,S*-NS₂C₇H₄)PR₃Ru{ κ^3 -*H,S,S'*-H₂B(NS₂C₇H₄)₂}], (*cis-fac-3a*: R = Cy; *cis-fac-3b*: R = Ph) along with complex *cis*-[(κ^2 -*N,S*-NS₂C₇H₄)₂Ru(PPh₃)₂], (*cis-4*). One of the main intentions of this study was to examine the flexibility of the borate and hemilabile *N,S*-chelating mercapto-benzothiazole ligands in adapting different spatial arrangements around metal center. Multinuclear spectroscopic analyses have been done to characterize all new complexes and the structures were further confirmed by single-crystal X-ray diffraction analysis. Further, Density Functional Theory (DFT) calculations were performed to provide an insight into the bonding of the complexes.

Introduction

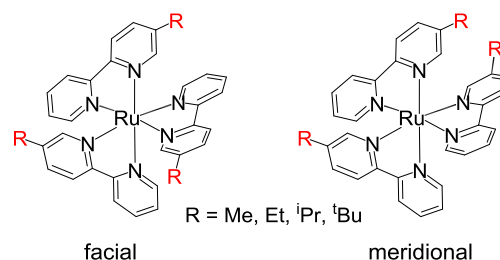
The synthesis and study of ruthenium complexes having boron-centered polyfunctional ligands have become a significant research interest over the past few decades.^[1] These polyfunctional ligands can stabilize the metal center with different coordination modes occupying preferred geometrical position. For example, Sabo-etienne *et al.* synthesized a phosphinobenzyl-(amino) borane ruthenium complex exhibiting two adjacent C-H and B-H agostic interactions that participate in selective B-H, C-H, and B-C bond activation.^[2] Recently, in many reports it have been found that borate ligands can show versatile coordination modes at ruthenium center,^[1a,3] where the metal center is stabilized by the 1,3-*N,S* donor ligand either in chelating (κ^2 -*N,S*) or in bridging (μ^2 -*N,S*/ μ^1 -*S*) coordination modes.^[1b,3,4,5] In fact, these 1,3-*N,S* chelated ligands have shown the potential hemilabile character to offer coordinative unsaturation at the metal center for further functionalization and to provide access to a large variety of functional groups with different steric and electronic properties.

The coordination chemistry of stable tridentate pincer-type ligands have also played an dominant role in catalysis owing to their ability to inhabit a particular coordination geometry in which the ligand occupies facial (*fac*) and meridional (*mer*) sites

a) κ^3 -*fac* and κ^3 -*mer* coordination geometries of Rhodium DPEphos Complexes



b) *fac* and *mer*-tris(bipyridine) complexes of ruthenium



c) Our work

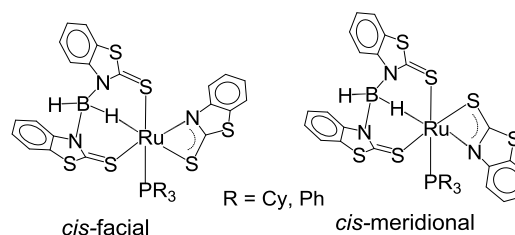


Chart 1. (a) *fac*- and *mer*-rhodium DPEphos complexes, (b) Examples of *fac*- and *mer*-ruthenium complexes, (c) *cis-mer* and *cis-fac* complexes, our work.

around metal center.^[6,7] For example, "POP" type ligands have been utilised in catalysis for decades, especially the ligand frameworks^[8,9] Xantphos or DPEphos [DPEphos = Bis{(2-diphenylphosphino)phenyl}ether] have been used in rhodium catalyzed hydroformylation reaction due to its wide bite angle.^[10] For example, Balakrishna and co-workers synthesized and structurally characterized DPEphos complex of ruthenium, *fac*-

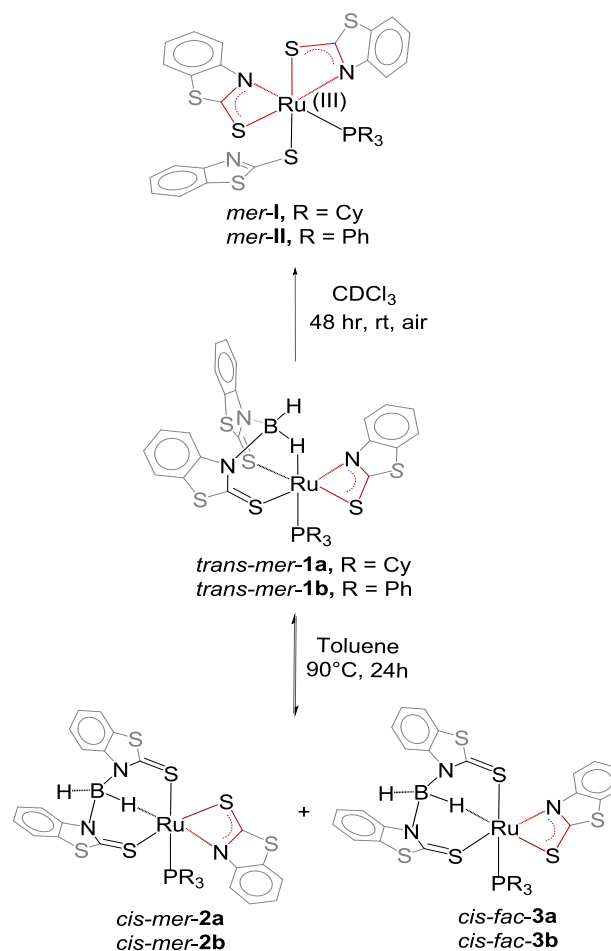
$[\text{Ru}(\text{S}(\text{O})\text{Me}_2)(\text{Cl})_2(\kappa^3\text{-P,O,P-DPEphos})]$ which upon addition of phosphine led to the formation of *mer*- $[\text{Ru}(\text{S}(\text{O})\text{Me}_2)(\text{Cl})_2(\kappa^3\text{-P,O,P-DPEphos})]$.^[11] Weller and co-workers reported rhodium complex, *fac*- $[\{\text{PCyp}_2(\eta^2\text{-C}_5\text{H}_7)\}\text{Rh}(\kappa^3\text{-P,O,P-DPEphos})][\text{BAR}^{\text{F}_4}]$ (Cyp = cyclopentanyl) which undergoes alkene hydrogenation in H_2 atmosphere to generate *fac*- $[\{\text{PCyp}_3\}\text{Rh}(\text{H})_2(\kappa^3\text{-P,O,P-DPEphos})][\text{BAR}^{\text{F}_4}]$ complex (Chart 1a).^[12a] Using cation-exchange chromatography, Fletcher and co-workers were able to isolate various new *fac*- and *mer*-isomers of 5-functionalized-2,2'-bipyridine complexes. The relative yield of the *fac* isomer was decreased significantly with increasing the steric bulk of the substituted group at 5-position of the bipyridine ligand (Chart 1b).^[12b]

The kinetic and thermodynamic stability of transition metal complexes with *cis-trans* facial and meridional stereoisomers are of considerable interest.^[13,14] According to theoretical studies, the *trans* isomers of these octahedral complexes are kinetically stable and they can be converted to *cis* form when subjected to thermolysis which has been further supported by the experimental studies.^[15] In the course of our recent studies on transition metal borate complexes, we have synthesized various $\kappa^2\text{-N,S}$ -chelated borate complexes *trans-mer*- $[(\kappa^2\text{-N,S-NS}_2\text{C}_7\text{H}_4)\text{PR}_3\text{Ru}\{\kappa^3\text{-H,S',S-H}_2\text{B}(\text{NS}_2\text{C}_7\text{H}_4)_2\}]$, (*trans-mer-1a*: R = PCy_3 , *trans-mer-1b*: R = PPh_3) and exploited their reactivity towards various small molecules such as boranes silanes, alkynes.^[16] While working on these $\kappa^2\text{-N,S}$ -chelated species, *trans-mer-1a-b*, we have observed that the aerial oxidation of these Ru(II) complexes generate redox-active Ru(III) species, *mer*- $[(\kappa^2\text{-N,S-NS}_2\text{C}_7\text{H}_4)_2\text{PR}_3\text{Ru}\{\kappa^1\text{-S}(\text{NS}_2\text{C}_7\text{H}_4)\}]$, (*mer-I*: R = PCy_3 , *mer-II*: R = PPh_3) (Scheme 1).^[17] This is mainly due to the hemilability of the $\kappa^2\text{-N,S}$ -chelated benzothiazole ligand coordinated to the ruthenium center. This observation prompted us to investigate the thermodynamic stability of *trans-mer-1a-b* at various temperatures. The main goal of this study was to examine the capability of the flexible borate moieties and hemilabile *N,S*-chelating mercaptobenzothiazolyl ligand to adopt different spatial arrangements at ruthenium center. Based on the coordination modes at the ruthenium center, we describe the novel isomerization reaction of *trans*-meridional to *cis*-meridional and *cis*-facial isomers of ruthenium borate species along with their electronic properties. To gain an insight into the electronic structure of the complexes, density functional theory (DFT) calculations were also carried out.

Results and Discussion

Thermolysis of *trans-mer-1a*. As shown in Scheme 1, room temperature aerial oxidation of *trans-mer-1a-b* in CDCl_3 converted to redox-active Ru(III) complexes, *mer-I-II*.^[17] However, when *trans-mer-1a* was thermolysed at 90°C for 24h, it led to the formation of **2a** and **3a** (Scheme 1). This reaction mixture did not benefit from thin-layer chromatographic (TLC) separation, which was attempted. This is mainly because of the fact that the species **2a** and **3a** are interconvertible in solution. Consequently, due to our inability to separate these complexes into their pure forms, we could not obtain pure spectral data for them. Therefore, we have attempted to fractionally crystallize **2a** and **3a** in order to isolate them in pure form. Fortunately, few needle-shaped yellow crystals were produced by a chloroform/hexane solution of **2a** and **3a** within the J-young

NMR tube which were identified as a $[(\kappa^2\text{-N,S-NS}_2\text{C}_7\text{H}_4)\text{PPh}_3\text{Ru}\{\kappa^3\text{-H,S,S'-H}_2\text{B}(\text{NS}_2\text{C}_7\text{H}_4)_2\}]$ **2a** that shows *cis-mer* geometry (Figure 1b).

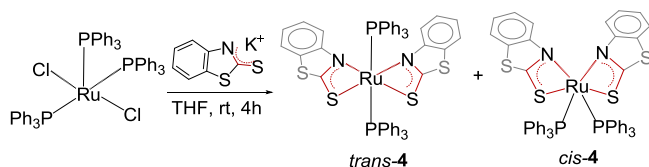


Scheme 1. Synthesis of the Ru(II) borate of complexes *cis-mer-2a-b*, *cis-fac-3a-b*.

Several attempts to get the crystals of **3a** were unsuccessful. As a result, in an attempt to get the analogous molecule of **3a**, we have carried out the thermolysis of *trans-mer-1b* that led to the formation of **2b** and **3b**, which are also under equilibrium. Fortunately, few needle-shaped yellow crystals were produced by a chloroform/hexane solution of **2b** and **3b** which were identified as a $[(\kappa^2\text{-N,S-NS}_2\text{C}_7\text{H}_4)\text{PPh}_3\text{Ru}\{\kappa^3\text{-H,S,S'-H}_2\text{B}(\text{NS}_2\text{C}_7\text{H}_4)_2\}]$ **3b** that shows *cis-fac* geometry, (Figure 1c).

In parallel to the formation of **2b** and **3b**, thermolysis of *trans-mer-1b* also yielded **4**. The $^{31}\text{P}\{^1\text{H}\}$ NMR spectrum of **4** displays a peak at $\delta = 52.3$ ppm. The ^1H NMR spectrum shows peaks in the aromatic region in the range of $\delta = 6.88\text{-}7.94$ ppm that denote the presence of two benzothiazole ligand and two phosphine ligands. The ESI-MS spectra of **4** shows peak at $m/z = 958.9921$ having isotopic distribution patterns. To get a clear picture for molecule **4**, single crystals appropriate for X-ray diffraction studies were grown from the slow diffusion of a CH_2Cl_2 /hexane solution at -5°C . Based on the X-ray diffraction studies along with the spectroscopic data, we have identified **4** as a *cis*- $[(\kappa^2\text{-N,S-C}_7\text{H}_4\text{NS}_2)_2\text{Ru}(\text{PPh}_3)_2]$ (*cis-4*, Figure 2, *vide infra*).^[18] Note that, in 2015, *cis-4* and *cis*- $[(\kappa^2\text{-N,S-$

$C_3H_4NS_2)_2Ru(PPh_3)_2$ complexes were isolated from the thermolysis of $[Ru(PPh_3)_3Cl_2]$ with 2-mercaptobenzothiazole and 2-mercaptobenzothiazoline, respectively in presence of NEt_3 and was characterized spectroscopically.^[19] In addition, earlier Sousa and co-workers isolated a series of analogous complexes with various heterocyclic bidentate ligands.^[20]



Scheme 2. Synthesis of *trans-4* and *cis-4*.

As complex *cis-4* turned out to be interesting and we have obtained solid-state X-ray structure, we wanted to make it in good quantity for further chemistry, in particular small molecule activation.^[16] Thus in an attempt to synthesize *cis-4* in a different route, one equivalent of $[Ru(PPh_3)_3Cl_2]$ was treated with two equivalents of potassium salt of 2-mercaptobenzothiazole ligand in THF at room temperature (Scheme 2). Within 4 hours, the colour of the reaction mixture changed from brown to yellow. The $^{31}P\{^1H\}$ NMR spectrum of the reaction mixture showed one peak at $\delta = 52.3$ ppm that corresponds to *cis-4* and the peak at $\delta = 41.6$ ppm indicates the formation of a new species *trans-4* (Figure S21). The mass spectrum of this reaction mixture displays a peak at $m/z = 958.9921$. The chromatographic separation of this mixture allowed us to isolate *cis-4* along with the unknown species, which was converted to *cis-4* over time. Systematic evaluation of multinuclear NMR spectroscopic data and mass spectrometric data of the reaction mixture suggested it as the isomer of the *cis-4*, that is *trans-4* (Figures S18–S21). Note that, thermolysis of *cis-4* at 90 °C for 24 hours does not show any conversion of *cis-4* to *trans-4*. Recently, we have reported redox-active complexes, *mer-I-II* that underwent unusual dual site B–H bond activation with boranes.^[16] Similarly, the presence of dual active sites in *cis-4* prompted us to explore the reactivity of it towards boranes. As shown in Scheme 3, the reaction of *cis-4* with $BH_3 \cdot THF$ at room temperature also led to the formation of *trans-mer-1b*.

X-ray crystallography and Geometry Assignment. As shown in Figures 1a–b, the solid state X-ray diffraction analyses of suitable crystals of **2a** and **3b** confirmed their molecular structures. Complex **2a** crystallizes in a triclinic system with space group $P\bar{1}$ and **3b** crystallizes in the monoclinic system with $P2_1/c$ space group. The molecular structure of **2a** shows a distorted octahedral geometry in which the tris-homoleptic mercaptobenzothiazolyl sulfur moieties are coordinated to the ruthenium center in meridional fashion. The phosphine is *cis* to the hydride ligand and the *N,S*-donor mercaptobenzothiazolyl ligand is coordinated to ruthenium that formed four-membered ruthenacycle with bite angle 67.60(11)°. Based on the coordination of the donor atoms to ruthenium center, **2a** now can be defined as *cis-mer-[(κ^2-N,S -NS₂C₇H₄)PCy₃Ru{ κ^3-H,S,S' -H₂B(NS₂C₇H₄)₂}]* (*cis-mer-2a*). The Ru1-S3 bond distance of 2.3217(14) Å in *cis-mer-2a* is significantly shorter than Ru1-S1 and Ru1-S5 bond distances of 2.4618(15) and 2.4396(14) Å, respectively. The Ru1-S1-C21-N1 ring is almost flat with a torsion angle of -0.7(5)° (Figures 1a).

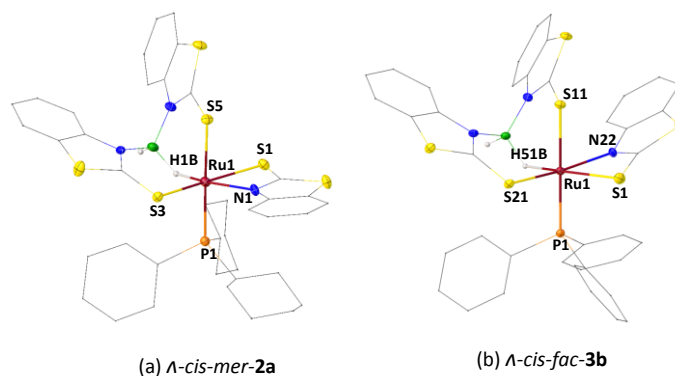
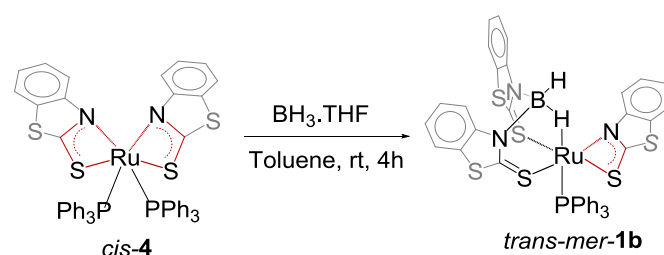


Figure 1. Molecular structures of *cis-mer-2a* (a), *cis-fac-3b* (b). Selected bond lengths (Å) and angles (°). *cis-mer-2a* (a): Ru1-B1 2.544(6), Ru1-P1 2.3485(14), Ru1-S1 2.4618(15), Ru1-S3 2.3217(14), Ru1-S5 2.4396(14), N1-Ru1-S1 67.60(11), S3-Ru1-S5 87.43(5), S3-Ru1-P1 94.46(5). *cis-fac-3b* (b): Ru1-B51 2.578(9), Ru1-P1 2.279(2), Ru1-N22 2.131(7), Ru1-S21 2.317(2), Ru1-S1 2.454(2), Ru1-S11 2.486(2), N22-Ru1-S1 67.6(2), S21-Ru1-S1 103.06(8), S21-Ru1-S11 87.37(17), S1-Ru1-S11 84.11(8).

The molecular geometries of **3b** depicted in Figures 1c revealed distorted octahedral geometry in which the mercaptobenzothiazolyl sulfur atoms are coordinated to ruthenium center in a facial fashion. However, the hydride, phosphine and nitrogen donor sites are *trans* to each of the mercaptobenzothiazolyl sulphur atoms. Four equatorial atoms of them are arranged in a square plane (H-S-S-N) and their structures are similar to *trans-mer-1b* with different orientation of the borate and phosphine ligand around ruthenium center. Interestingly, in both the cases, the hydride ligand is *cis*-oriented to the phosphine ligand. Three sulfur atoms of tris-homoleptic mercaptobenzothiazolyl are coordinated to the ruthenium center in facial fashion. As a result of the donor atoms coordination with the ruthenium centre, **3b** may now be described as *cis-fac-3b*. The bite angles (N-Ru-S) for four membered chelating ruthenacycle are 67.6(2)° for *cis-fac-3b*. The Ru-B bond distance of 2.575(3) Å (*cis-fac-3b*) are comparatively shorter as compared to *trans-mer-1b* (2.775 Å). The Ru-P bond distances for *cis-fac-3b* (2.2740(7)Å) are significantly longer as compared to *trans-mer-1b* 2.2696(15) Å.



Scheme 3. Synthesis of *trans-mer-1b* from *cis-4*.

The molecular structure of **4**, shown in Figure 2, displays an octahedral geometry around Ru center comprising two $\kappa^2-1,3-N,S$ -chelated rings along with two phosphine ligands. Considering the fact that these phosphine ligands are *cis* to each other, **4** is defined as *cis-4*. In addition, the phosphine ligands are *trans* to the N atoms of the $\kappa^2-1,3-N,S$ -mercaptobenzothiazolyl donor ligands. The torsion angles of both the four-membered (S-C-N-Ru) rings (1.6(6)° and -0.4(6)°

match well with that of *trans-mer-1b* ($0.9(4)^\circ$). The Ru-S distances of 2.433(3) Å and 2.450(3) Å in the chelate rings are comparable with that of *trans-mer-1b* (2.4741(18) Å).

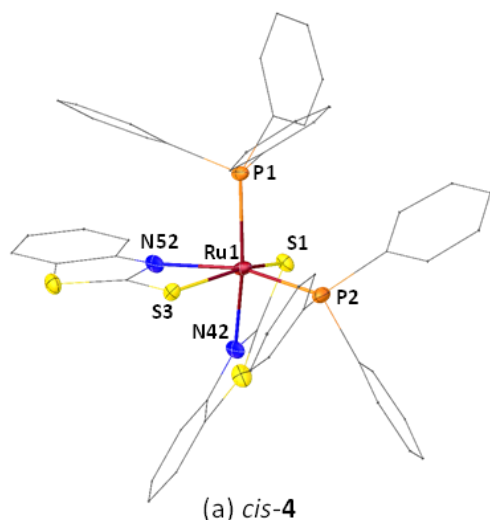


Figure 2. Molecular structures of *cis-4* (a), selected bond lengths (Å) and angles ($^\circ$). *cis-4*: Ru1-P1 2.300(3), Ru1-P2 2.301(3), Ru1-S1 2.433(3), Ru1-S3 2.450(3), Ru1-N42 2.177(10), N42-Ru1-S1 67.3(3) N52-Ru1-S3 67.1(3).

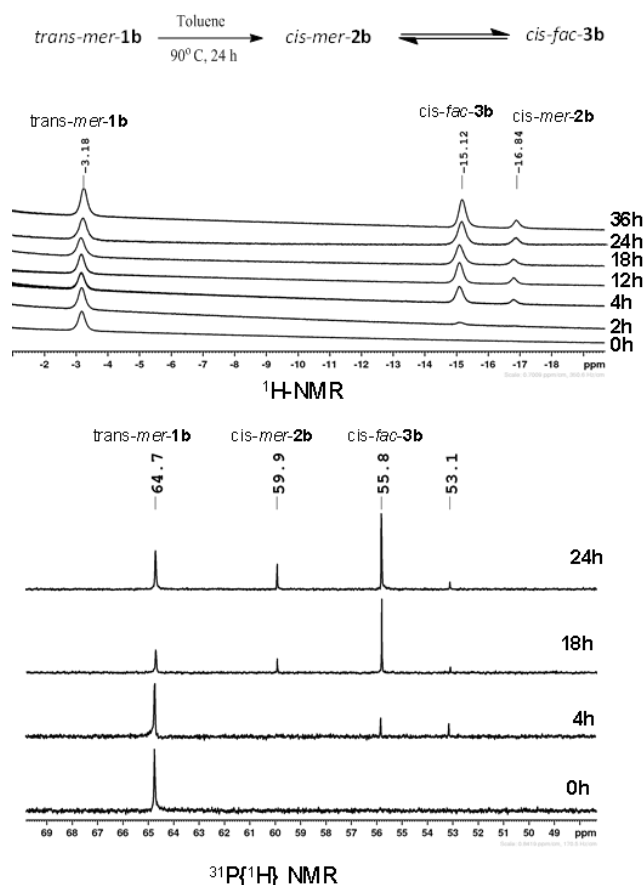


Figure 3. ^1H and $^{31}\text{P}\{^1\text{H}\}$ NMR studies for interconversion of *trans-mer-1b* to *cis-mer-2b* and *cis-fac-3b*.

***cis-trans* Orientation of the Hydride.** As discussed above, thermolysis of *trans-mer-1a-b* yielded *cis-mer-2a-b* and *cis-fac-3a-b*. Having all these molecules with different phosphines, we are now able to assign the ^1H , $^{11}\text{B}\{^1\text{H}\}$ and $^{31}\text{P}\{^1\text{H}\}$ chemical shifts from their combined NMR spectra. The $^{11}\text{B}\{^1\text{H}\}$ NMR spectrum of the mixture of **2b** and **3b** shows one broad resonance in the upfield region at $\delta = -4.6$ ppm. Besides the ^1H chemical shifts for mercaptobenzothiazolyl and phosphine ligands, the ^1H NMR spectra of them show chemical shifts in the range of $\delta = -16.84$ to -15.12 ppm likely due to the presence of Ru-H-B protons. In *cis-mer-2b*, the hydride is trans to N, whereas in case of *cis-fac-3b*, the hydride is trans to S atom. Due to the greater electronegativity of N atom, donation of electrons from the B-H bond to ruthenium is expected to be more as compared to the Ru-H-B proton, which is trans to S atom. As a result, it is reasonable to assume that the metal hydride character for Ru-H-B proton in *cis-mer-2b* is greater than the *cis-fac-3b* isomer. Thus, the ^1H chemical shift of the hydride in *cis-mer-2b* appears in the upfield region as compared to *cis-fac-3b*. Based on the trans effect and DFT studies (Table S1), the peak at $\delta = -16.84$ ppm is assigned to Ru-H-B of *cis-mer-2b* and the chemical shift at $\delta = -15.12$ ppm is allocated to *cis-fac-3b* (Figure 3). The ^{31}P chemical shifts at $\delta = 55.8$ ppm has been assigned to *cis-fac-3b* and $\delta = 59.9$ ppm for *cis-mer-2b* (Table S1). An ESI-MS spectrum shows an isotropic pattern at m/z 874.9563. In a similar fashion, the chemical shifts for *cis-mer-2a* and *cis-fac-3a* have been assigned (Figures S4-S17).

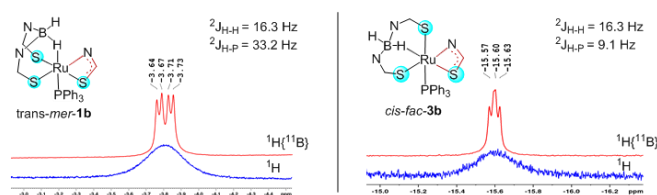


Figure 4. Comparison of ^1H and $^{11}\text{B}\{^1\text{H}\}$ NMR spectrum for *trans-mer-1b* and *cis-fac-3b*.

The *cis-trans* nomenclature for molecules *trans-mer-1a-b*, *cis-mer-2a-b*, and *cis-fac-3a-b*, has been established based on the $J(\text{H},\text{P})$ coupling constant values obtained from $^{11}\text{B}\{^1\text{H}\}$ NMR. In the ^1H NMR spectrum for *trans-mer-1b*, the broad hydride peak at $\delta = -3.71$ ppm appeared as a doublet of doublet when decoupled with ^{11}B ($^2J_{\text{HP}} = 33.2$ Hz, $^2J_{\text{HH}} = 16.3$ Hz) (Figure 4). This indicates that the hydride is trans to phosphine ligand.^[21] Similarly, for *cis-fac-3b*, the broad hydride peak at $\delta = -15.6$ ppm appears as a doublet of doublet with coupling constants, $^2J_{\text{HP}} = 9.1$ Hz and $^2J_{\text{HH}} = 16.3$ Hz. This may be due to the adjacent *cis*-oriented phosphine group. This looks like a triplet as a consequence of minimal difference in coupling constant values of $^2J_{\text{HP}}$ and $^2J_{\text{HH}}$. The ^1H NMR spectra for *cis-mer-2b* and *cis-fac-3b* appeared significantly in the upfield region as compared to *trans-mer-1b* ($\delta = -3.4$ ppm). This is due to the trans effect of the phosphine ligands. The ^1H chemical shift of the aromatic protons of 1,3-*N,S*-chelated mercaptobenzothiazole ligand of *cis-fac-3b* has been shifted significantly to upfield region as compared to *trans-mer-1b* isomer. This may be due to the *cis* orientation of the phosphine moiety.^[22]

DFT Calculations. To gain some insight into the bonding nature and to understand the differences and similarities of the *trans-mer-1a-1b*, *cis-mer-2a*, *cis-fac-3a* stereoisomers, various computational simulations at the bp86/def2-tzvp^[23] level of theory-based in DFT were executed. The HOMOs of the *trans* isomers are mainly localized on the d-orbital of ruthenium and the p-orbitals of nitrogen and sulfur atoms of the borate ligand, whereas in the case of the *cis* isomers, the HOMOs involve the p-orbitals of sulfur atoms of the chelated benzothiazole moiety along with the ruthenium d-orbital and p-orbitals nitrogen and sulfur atoms of the borate ligand (Figure S23). The LUMOs are mainly found to be localized over benzothiazole moieties of borate ligand for both the isomers (Figure S23). The HOMO-LUMO energy gap increases in the order *trans-mer* < *cis-fac* < *cis-mer* (Table S2). The natural bonding orbital (NBO) analysis shows that charge transfer from phosphorus to ruthenium follows the trend *trans-mer* < *cis-mer* < *cis-fac*,^[24] which is further supported by the natural valence population analysis (Table S2).

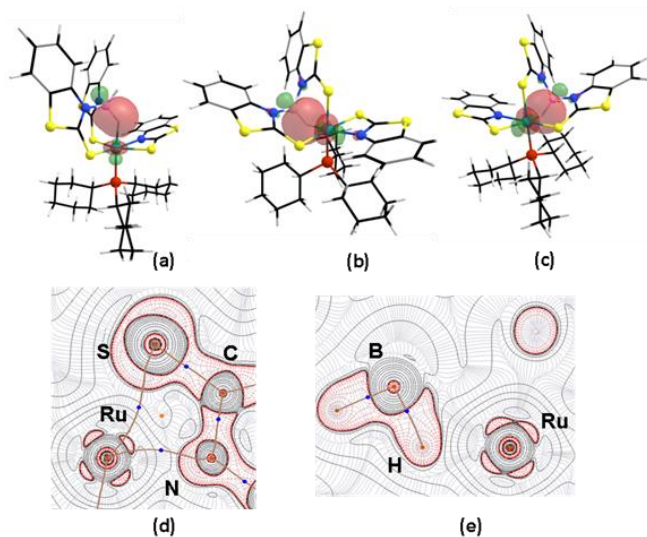


Figure 5. (a), (b) and (c) represents the Ru-H-B interaction in *trans-mer-1a*, *cis-mer-2a* and *cis-fac-3a* respectively; (d) and (e) shows the Contour-line map of the Laplacian of the electron density in the Ru-SCN plane and Ru-H-B plane of *cis-mer-2a*. BCPs and RCPs correspond to blue and orange dots and red lines indicate bond paths.

The NBO analysis dictates very strong Ru-H-B bonding interaction (Figure 5a-c). In addition, the contour plot of the laplacian of the electron density ($\nabla^2\rho$) shows the presence of a ring-critical point (RCP) in the RuSCN plane of *cis-mer-2a* (Figure 5d).

Electronic spectra. Conversion of *trans-mer-1a-b* to *cis-mer-2a-b* and *cis-fac-3a-b* has prompted us to explore the photo-physical properties of these isomers. The UV-vis spectra of complexes **1a-3a** and **1b-3b** recorded in dichloromethane shows an intense absorption band in the region of 236-250 nm that may be assigned to $\pi-\pi^*$ transitions of the phosphine and mercaptobenzothiazolyl ligands (Figure 6). Another electronic transition peak in the window of 317-421 nm is possibly due to the charge transfer transition (MLCT). The results indicate that the ligands orientation around the metal center does not significantly affect the general photo-physical properties of the complexes.

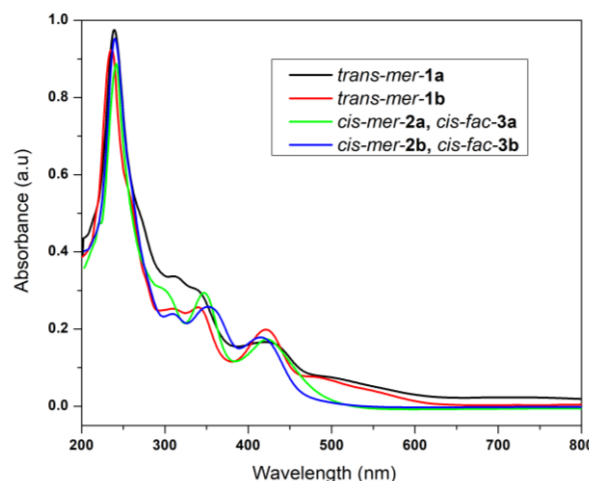


Figure 6. UV-vis spectra of *trans-mer-1a-b*, *cis-mer-2a-b* and *cis-fac-3a-b*.

Cyclic voltammetry. Lahiri, Liobet and coworkers have demonstrated that one may compare the electron density on the central metal atom provided by the ligand that is arranged in *trans* and *cis* fashion around the metal centre by using cyclic voltammetry as a tool.^[25] These observations encourage us to conduct cyclic voltammetry experiment. The redox behaviour of *trans-mer-1b*, and mixture of *cis-mer-2b*, *cis-fac-3b* species has been studied by cyclic voltammetry (CV). The voltammograms of both compounds are almost similar; the main difference observed is the peak potentials. The cyclic voltammogram for *trans-mer-1b* in dichloromethane shows reversible waves at $E_{1/2} = 0.47$ V, ($I_{pc}/I_{pa} = 0.97$) and for *cis-fac-3b* the reversible peaks appear at 0.59 V ($I_{pc}/I_{pa} = 0.98$), (Figure S22) respectively. These peaks have been assigned to Ru^{III}/Ru^{II} redox couple. In addition, the irreversible waves at 0.79 V (*trans-mer-1b*) and 0.93 V (*cis-fac-3b*) appears due to oxidation of the *N,S*-donor mercaptobenzothiazole redox centered couple. With reference to their respective positions, the phosphine and hydride ligands provided a higher electron density on the ruthenium metal enabling the *cis-mer-2b*, *cis-fac-3b* anodic peak to arise at a higher potential than the *trans-mer-1b* anodic peak. This makes *trans* isomer more capable of oxidising the metal centre than *cis* isomers. As a result, the oxidation potential emerges at a lower value for the *trans* isomer.

Conclusion

In summary, we have synthesized some interesting *cis-meridional* and *cis-facial* isomers of ruthenium borate species which are supported by hemilabile *N,S*-chelated ruthenacycle. They are exciting stereoisomeric organometallic species, based on a *cis-trans* isomer they might open a new direction in catalysis. Further, we have studied the kinetic and thermodynamic stability of these stereoisomers of ruthenium borate complexes at different reaction conditions. In addition, we have synthesized *cis-trans* isomeric mixture of stereoisomers in which the octahedral Ru centre is coordinated with two units of chelate ring through 1,3-*N,S*-chelating fashion along with two phosphine moieties. Based on the J(H,P) coupling constant values obtained from boron decoupled proton NMR, the *cis-trans* nomenclature for the molecules *trans-mer-1a-b*, *cis-mer-2a-b*, and *cis-fac-3a-b* has been defined. Comparative study of *cis* and *trans* isomer on the basis of different in electron density

on the central metal has been demonstrated by cyclic voltammetry. Selective synthesis of these type of complexes open the pathways towards the activation of small molecules and their interesting prospect in catalysis are currently being explored.

Experimental Section

General Procedures and Instrumentation. All operations were done by using glove box techniques and standard Schlenk line under an atmosphere of dry argon. Solvents such as tetrahydrofuran, hexane and toluene were distilled through Na/benzo-phenoneketyl and dichloromethane was dried over calcium hydride prior to use under argon. CDCl_3 dried over calcium hydride for 12 h, and degassed by three freeze-pump-thaw cycles, stored over 4 Å molecular sieves in a Young's ampoule under argon. The complexes $[\text{R}_3\text{P}(\kappa^2\text{-}N,S\text{-}(\text{C}_7\text{H}_4\text{NS}_2))\text{Ru}(\kappa^3\text{-}H,S,S'\text{-}H_2\text{B}(\text{C}_7\text{H}_4\text{NS}_2)_2)]^{16b}$ (**1a**: R = Cy; **1b**: R = Ph), $[\text{Ru}(\text{PPh}_3)_3\text{Cl}_2]^{26}$ was prepared according to literature. The external reference for the $^{11}\text{B}\{^1\text{H}\}$ NMR spectroscopy, $[\text{Bu}_4\text{N}][(\text{B}_3\text{H}_6)]^{27}$ was synthesized according to the literature method. The ^1H , $^1\text{H}\{^{11}\text{B}\}$, $^{11}\text{B}\{^1\text{H}\}$, $^{13}\text{C}\{^1\text{H}\}$, and $^{31}\text{P}\{^1\text{H}\}$ were recorded on Bruker 400 and 500 MHz instruments. The residual solvent protons were used as reference (δ , ppm, Benzene- d_6 , 7.16, CDCl_3 , 7.26, Toluene- d_6 , 7.09 ppm), while as an external reference for ^{11}B NMR spectra, a sealed tube containing $[\text{Bu}_4\text{N}][(\text{B}_3\text{H}_6)]$ in Benzene- d_6 (δ , ppm, -30.07) was used. To remove the broad ^{11}B background signal of the NMR tube, ^1H decoupled ^{11}B spectra of all compounds were administered with a backward linear prediction algorithm. Aluminum supported silica gel TLC plates with 250 μm diameter (Merck TLC plates) were utilized in thin layer chromatographic separation of the reaction mixture. High-resolution ESI-MS were recorded with an Agilent 6545A Q-TOF mass spectrometer. Infrared spectra were obtained on a Jasco FT/IR-1400 spectrometer.

Please see synthetic procedures and experimental details in Supporting information.

X-ray structure analysis. Suitable X-ray quality crystals of *cis-fac-3b* and *cis-4* were grown by slow diffusion of a hexane/dichloromethane solution at -5°C , respectively. Whereas the crystals of *cis-mer-2a* were grown by slow diffusion of a chloroform/hexane at -33°C . Crystal data of *cis-mer-2a*, *cis-fac-3b* and *cis-4* were obtained using a D_8 VENTURE Bruker SC diffractometer with graphite monochromated Mo-K α ($\lambda = 0.71073$ Å) radiation at 150 (2) K. All the structures were solved using SIR97^[28] and refined with SHELXL-2018, SHELXL-2014, and SHELXL-2017.^[29] Using Olex2^[30] all the molecular structures were drawn. The non-hydrogen atoms were refined with anisotropic displacement parameters. All hydrogens could be located in the difference Fourier map. However, the hydrogen atoms bonded to carbon and boron atoms were fixed at chemically meaningful positions and were allowed to ride with the parent atom during the refinement. Crystallographic data have been deposited with the Cambridge Crystallographic Data Center as supplementary publication no CCDC-2052114 (for *cis-mer-2a*), CCDC-2052098 (for *cis-fac-3b*), CCDC-1588903 (for *cis-4*). These data can be obtained free of charge from The Cambridge Crystallographic Data Centre via www.ccdc.cam.ac.uk/data_request/cif.

Crystal data for *cis-mer-2a*: $\text{C}_{41}\text{H}_{49}\text{BN}_3\text{PRuS}_6$, $M_r = 1131.74$ triclinic, space group $P\bar{1}$, $a = 9.6800(9)$ Å, $b = 14.8343(15)$ Å, $c = 17.6279(19)$ Å, $\alpha = 106.423(4)^\circ$, $\beta = 90.327(3)^\circ$, $\gamma = 96.470(3)^\circ$, $V = 2410.7(4)$ Å³, $Z = 2$, $\rho_{\text{calcd}} = 1.559$ g/cm³, $\mu = 0.542$ mm⁻¹, $F(000) = 1156$, $R_1 = 0.0684$, $wR_2 = 0.1814$, 10686 independent reflections [$2\theta \leq 50.484^\circ$] and 551 parameters.

Crystal data for *cis-fac-3b*: $\text{C}_{39}\text{H}_{29}\text{BN}_3\text{PRuS}_6$, $M_r = 874.86$, monoclinic, space group $P2_1/c$, $a = 10.9746(9)$ Å, $b = 23.0317(17)$ Å, $c = 14.6758(12)$ Å, $\alpha = 90^\circ$, $\beta = 103.997(3)^\circ$, $\gamma = 90^\circ$, $V = 3599.4(5)$ Å³, $Z = 4$,

$\rho_{\text{calcd}} = 1.614$ g/cm³, $\mu = 0.864$ mm⁻¹, $F(000) = 1776$, $R_1 = 0.0357$, $wR_2 = 0.0925$, 8231 independent reflections [$2\theta \leq 55.038^\circ$] and 466 parameters.

Crystal data for *cis-4*: $\text{C}_{50}\text{H}_{38}\text{N}_2\text{P}_2\text{RuS}_4$, $M_r = 958.07$, monoclinic, space group $P2_1/c$, $a = 24.831(4)$ Å, $b = 16.766(3)$ Å, $c = 22.551(4)$ Å, $\alpha = 90^\circ$, $\beta = 95.561(6)^\circ$, $\gamma = 90^\circ$, $V = 9344(3)$ Å³, $Z = 8$, $\rho_{\text{calcd}} = 1.362$ g/cm³, $\mu = 0.619$ mm⁻¹, $F(000) = 3920.0$, $R_1 = 0.1595$, $wR_2 = 0.3902$, 21342 independent reflections [$2\theta \leq 54.968^\circ$] and 977 parameters.^[17]

Computational Details. Density functional theory (DFT) calculations employing BP86^[23] functional were performed with the Gaussian 16^[31] program. Full geometry optimizations were conducted in gaseous state (no solvent effect) without any symmetry constraints using a def2-tzvp basis set from Basis Set Exchange Library.^[32] The optimized geometries were characterized as true minima by conducting frequency calculations. We have computed ^{11}B NMR chemical shifts using gauge-including atomic orbitals (GIAOs)^[33] method at the same basis set by B3LYP. The ^{11}B NMR chemical shifts were calculated relative to B_2H_6 and converted to the usual $[\text{BF}_3\cdot\text{OEt}_2]$ scale by using experimental δ (^{11}B) value of B_2H_6 ($\delta = 16.6$ ppm).^[34] Natural bonding analyses were carried out with the natural bond orbital (NBO) 6.0 version of program.^[35] Wiberg bond indices (WBI)^[36] were obtained from natural bond orbital analysis. The electron density and Laplacian electronic distribution plots were generated using Multiwfn package.^[37] All the optimized structures and orbital plots were generated by using Chemcraft.^[38]

Acknowledgements

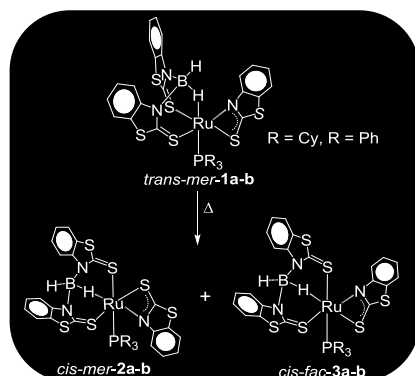
This work was supported by Council of Scientific & Industrial Research (CSIR) (Scheme No. 01(3055)/21/EMR-II), New Delhi, India. A. A thanks Council of Scientific & Industrial Research (CSIR) and S. S. thanks INSPIRE for research fellowship. M. Z. thank IIT Madras for research fellowship. IIT Madras is gratefully acknowledged for computational facilities.

Keywords: borate • facial • isomerism • meridional • ruthenium

- [1] a) S. Saha, F. Assanar, S. Ghosh, *Eur. J. Inorg. Chem.* **2022**, e202200587; b) K. Saha, D. K. Roy, R. D. Dewhurst, S. Ghosh, H. Braunschweig, *Acc. Chem. Res.* **2021**, *54*, 1260–1273; c) U. Kaur, K. Saha, S. Gayen, S. Ghosh, *Coord. Chem. Rev.* **2021**, *446*, 214106–214130; d) I. Kuzu, I. Krummenacher, J. Meyer, F. Armbruster, F. Breher, *Dalton Trans.* **2008**, 5836–5865; e) P. Braunstein, *J. Organomet. Chem.* **2004**, *689*, 3953–3967; f) R. H. Crabtree, *New J. Chem.* **2001**, *35*, 18–23.
- [2] A. Cassen, Y. Gloaguen, L. Vendier, C. Duhayon, A. P. Bahamonde, C. Raynaud, E. Clot, G. Alcaraz, S. Sabo-Etienne, *Angew. Chem. Int. Ed.* **2014**, *53*, 7569–7577; *Angew. Chem.* **2014**, *126*, 7699–7703.
- [3] a) M. Paneque, S. Sirol, M. Trujillo, E. Gutierrez-Puebla, M. A. Monge, E. Carmona, *Angew. Chem. Int. Ed.* **2000**, *39*, 218–222; *Angew. Chem.*, **2000**, *112*, 224–227; b) D. K. Roy, B. Mondal, R. S. Anju, S. Ghosh, *Chem. Eur. J.* **2015**, *21*, 3640–3648; c) R. S. Anju, D. K. Roy, K. Geetharani, B. Mondal, B. Varghese, S. Ghosh, *Dalton Trans.* **2013**, *42*, 12828–12831; d) R. Borthakur, K. Saha, S. Kar, S. Ghosh, *Coord. Chem. Rev.* **2019**, *399*, 213021–213037; e) K. Saha, U. Kaur, S. Kar, B. Mondal, B. Joseph, P. K. S. Antharjanam, S. Ghosh, *Inorg. Chem.* **2019**, *58*, 2346–2353.
- [4] R. Ramalakshmi, K. Saha, D. K. Roy, B. Varghese, A. K. Phukan, S. Ghosh, *Chem. Eur. J.* **2015**, *21*, 17191–17195.
- [5] K. Saha, R. Ramalakshmi, S. Gomosta, K. Pathak, V. Dorcet, T. Roisnel, J. Halet, S. Ghosh, *Chem. Eur. J.* **2017**, *23*, 9812–9820.
- [6] A. F. Moneris, K. Magra, M. Darari, C. Cebrían, M. Beley, E. Domenichini, S. Haacke, M. Pastore, X. Assfeld, P. C. Gros, A. Monari, *Inorg. Chem.* **2018**, *57*, 10431–10441.

- [7] a) M. A. Esteruelas, C. García-Yebra, J. Martín, E. Oñate, *Inorg.Chem.* **2017**, *56*, 676–683; b) S. Arroliga-Rocha, D. Escudero, *Inorg. Chem.* **2018**, *57*, 12106–12112; c) A. B. Tamayo, B. D. Alleyne, P. I. Djurovich, S. Lamansky, I. Tsyba, N. N. Ho, R. Bau, M. E. Thompson, *J. Am. Chem. Soc.* **2003**, *125*, 7377–7387.
- [8] C. Gunanathan, D. Milstein, *Acc. Chem. Res.* **2011**, *44*, 588–602.
- [9] a) G. van Koten, *Top. Organomet. Chem.*, **2013**, *40*, 1–20; b) D. Morales-Morales, C. Jensen, *The Chemistry of Pincer Compounds*, Elsevier, Amsterdam, **2007**.
- [10] M. Kranenburg, Y.E.M. van der Burgt, P.C.J. Kamer, P.W.N.M. van Leeuwen, K. Goubitz, J. Fraanje, *Organometallics* **1995**, *14*, 3081–3089.
- [11] R. Venkateswaran, J. T. Mague, M. S. Balakrishna, *Inorg. Chem.* **2007**, *46*, 809–817.
- [12] a) R. Dallanegra, A. B. Chaplin, A. S. Weller, *Organometallics*, **2012**, *31*, 2720–2728; b) M. Nieuwenhuyzen, S. Rainey, N. C. Fletcher, *J. Chem. Soc., Dalton Trans.* **2001**, 2641–2648.
- [13] a) L. Salassa, C. Garino, G. Salassa, R. Gobetto, C. Nervi, *J. Am. Chem. Soc.* **2008**, *130*, 9590–9597; b) L. Salassa, E. Borfecchia, T. Ruiu, C. Garino, D. Gianolio, R. Gobetto, P. J. Sadler, M. Cammarata, M. Wulff, C. Lamberti, *Inorg. Chem.* **2010**, *49*, 11240–11248; c) A. Poater, F. Ragone, A. Correa, A. Szadkowska, M. Barbasiewicz, K. Grell, L. Cavallo, *Chem. Eur. J.* **2010**, *16*, 14354–1436.
- [14] N. C. Fletcher; M. Nieuwenhuyzen; R. Prabakaran; A. Wilson, *Chem. Commun.* **2002**, 1188.
- [15] Y. Luo.; P. G. Potvin.; Y. Tse; A. B. P. Lever, *Inorg. Chem.* **1996**, *35*, 5445.
- [16] a) M. Zafar, R. Ramalakshmi, A. Ahmad, P. K. S. Antharjanam, S. Bontemps, S. Sabo-Etienne, S. Ghosh, *Inorg. Chem.* **2021**, *60*, 1183–1194; b) M. Zafar, R. Ramalakshmi, K. Pathak, A. Ahmad, T. Roisnel, S. Ghosh, *Chem. Eur. J.* **2019**, *25*, 13537–13546.
- [17] M. Zafar, A. Ahmad, S. Saha, R. Ramalakshmi, T. Roisnel, S. Ghosh, *Chem.Sci.* **2022**, *13*, 8567–8575.
- [18] Note that the characterization of *cis-4* was solely based on its spectroscopic data. Thus, in an attempt to get the structural details of *cis-4*, we have carried out X-ray diffraction studies with a very poor crystal. Several attempts to get a good quality crystal for *cis-4* were failed.
- [19] P. Appelt, F. D. Fagundes, G. Facchin, M. G. Kramer, D. F. Back, M. A. A. Cunha, B. Sandrino, K. Wohnrath, M. P. de Araujo, *Inorg. Chim. Acta* **2015**, *436*, 152–158.
- [20] A. Sousa-Pedrares, M. Luz Durán, J. Romero, J.A. García-Vázquez, J.C. Monteagudo, A. Sousa, J.R. Dilworth, *Inorg. Chim. Acta.* **2006**, *359*, 863–876.
- [21] a) Y. Gloaguen, G. Alcaraz, A-F. Péharman, E. Clot, L. Vendier, S. Sabo-Etienne, *Angew. Chem. Int. Ed.* **2009**, *48*, 2964–2968; *Angew. Chem.* **2009**, *121*, 3008–3012; b) G. Alcaraz, L. Vendier, E. Clot, S. Sabo-Etienne, *Angew. Chem. Int. Ed.* **2010**, *49*, 918–920; *Angew. Chem.* **2010**, *122*, 930–932.
- [22] K. D. Spielvogel, J. A. Luna, S. M. Loria, L. P. Weisburn, N. C. Stumme, M. R. Ringenberg, G. Durgaprasad, J. M. Keith, S. K. Shaw, S. R. Daly, *Inorg. Chem.*, **2020**, *59*, 10845–10853.
- [23] A. D. Becke, *Phys. Rev. A* **1988**, *38*, 3098–3100; b) J. P. Perdew, *Phys. Rev. B.* **1986**, *33*, 8822–8824; c) A. Schäfer, C. Huber; R. Ahlrichs, *J. Chem. Phys.* **1994**, *100*, 5829–5235.
- [24] W. Drescher, D. Schmitt-Monreal, C. R. Jacob, C. Kleeberg, *Organometallics* **2020**, *39*, 538–543.
- [25] M. A. Hoque, A. D. Chowdhury, S. Maji, J. Benet-Buchholz, M. Z. Ertem, C. Gimbert-Surinach, G. K. Lahiri, A. Llobet, *Inorg.Chem.* **2021**, *60*, 5791–5803.
- [26] P.S. Hallman, T.A. Stephenson, G. Wilkinson, *Inorg. Synth.*, R.W. Parry (Ed.), **1970**, pp. 237–240.
- [27] G.E. Ryschkewitsch, K.C. Nainan, *Inorg. Synth.* **1974**, *15*, 113–114.
- [28] (a) G. M. Sheldrick, *Acta Cryst.* **2015**, *A71*, 3–8. (b) G. M. Sheldrick, SHELXS97 and SHELXL97, University of Göttingen: Germany, 1997.
- [29] G. M. Sheldrick, *Acta Cryst.* **2015**, *C71*, 3–8.
- [30] O. V. Dolomanov, L. J. Bourhis, R. J. Gildea, J. A. K. Howard, H. Puschmann, *J. Appl. Crystallogr.*, **2009**, *42*, 339–341.
- [31] Gaussian 16, Revision B.01, M. J. Frisch, G. W. Trucks, H. B. Schlegel, G. E. Scuseria, M. A. Robb, J. R. Cheeseman, G. Scalmani, V. Barone, G. A. Petersson, H. Nakatsuji, X. Li, M. Caricato, A. V. Marenich, J. Bloino, B. G. Janesko, R. Gomperts, B. Mennucci, H. P. Hratchian, J. V. Ortiz, A. F. Izmaylov, J. L. Sonnenberg, D. Williams-Young, F. Ding, F. Lipparini, F. Egidi, J. Goings, B. Peng, A. Petrone, T. Henderson, D. Ranasinghe, V. G. Zakrzewski, J. Gao, N. Rega, G. Zheng, W. Liang, M. Hada, M. Ehara, K. Toyota, R. Fukuda, J. Hasegawa, M. Ishida, T. Nakajima, Y. Honda, O. Kitao, H. Nakai, T. Vreven, K. Throssell, J. A. Jr. Montgomery, J. E. Peralta, F. Ogliaro, M. J. Bearpark, J. J. Heyd, E. N. Brothers, K. N. Kudin, V. N. Staroverov, T. A. Keith, R. Kobayashi, J. Normand, K. Raghavachari, A. P. Rendell, J. C. Burant, S. S. Iyengar, J. Tomasi, M. Cossi, J. M. Millam, M. Klene, C. Adamo, R. Cammi, J. W. Ochterski, R. L. Martin, K. Morokuma, O. Farkas, J. B. Foresman, D. J. Fox, Gaussian, Inc., Wallingford CT, **2016**.
- [32] Basis Set Exchange Library. <https://www.basissetexchange.org/>
- [33] (a) F. J. London, *J. Phys. Radium* 1937, *8*, 397–409, (b) R. Ditchfield, *Mol. Phys.* **1974**, *27*, 789–807, (c) K. Wolinski, J. F. Hinton, P. Pulay, *J. Am. Chem. Soc.* **1990**, *112*, 8251–8260.
- [34] T. P. Onak, H. L. Landesman, R. E. Williams, I. Shapiro, *J. Phys. Chem.* **1959**, *63*, 1533–1535.
- [35] NBO Program 6.0, E. D. Glendening, J. K. A. E. Badenhop, Reed, J. E. Carpenter, J. A. Bohmann, C. M. Morales, C. R. Landis and F. Weinhold, Theoretical Chemistry Institute, University of Wisconsin, Madison, WI, **2013**.
- [36] K. Wiberg, *Tetrahedron* **1968**, *24*, 1083–1096.
- [37] T. Lu, F. Chen, Multiwfn: A multifunctional wavefunction analyzer. *J. Comput. Chem.* **2012**, *33*, 580–592.
- [38] Chemcraft - graphical software for visualization of quantum chemistry computations <https://www.chemcraftprog.com>.

Entry for the Table of Contents



The *cis-mer*- and *cis-fac*- κ^2 -*N,S*-chelated ruthenium borate complexes have been synthesised from the thermolysis of *trans-mer* isomers. The hemilability of the flexible borate ligand is one of the key factors for the formation of these isomers.